Cellular/Molecular

βIV Spectrins Are Essential for Membrane Stability and the Molecular Organization of Nodes of Ranvier

Yang Yang,[1] Sandra Lacas-Gervais,[2] D. Kent Morest,[1] Michele Solimena,[2] and Matthew N. Rasband[1]

[1]Department of Neuroscience, University of Connecticut Health Center, Farmington, Connecticut 06030-3401, and [2]Medical School, Technical University Dresden, 01307 Dresden, Germany

High densities of sodium channels at nodes of Ranvier permit action potential conduction and depend on βIV spectrins, a family of scaffolding proteins linked to the cortical actin cytoskeleton. To investigate the molecular organization of nodes, we analyzed qv^{3J} "quivering" mice, whose βIV spectrins have a truncated proline-rich "specific" domain (SD) and lack the pleckstrin homology (PH) domain. Central nodes of qv^{3J} mice, which lack βIV spectrins, are significantly broader and have prominent vesicle-filled nodal membrane protrusions, whereas axon shape and neurofilament density are dramatically altered. PNS qv^{3J} nodes, some with detectable βIV spectrins, are less affected. In contrast, a larger truncation of βIV spectrins in qv^{4J} mice, deleting the SD, PH, and ankyrinG binding domains, causes βIV spectrins to be undetectable and causes dramatic changes, even in peripheral nodes. These results show that quivering mutations disrupt βIV spectrin retention and stability at nodes and that distinct protein domains regulate nodal structural integrity and molecular organization.

Key words: **Na^+ channel; cytoskeleton; axon–glia interaction; myelin; node of Ranvier; axon**

Introduction

Nodes of Ranvier and axon initial segments (AISs) are characterized by high-density clusters of voltage-gated Na^+ (Nav) channels that are essential for the generation and propagation of action potentials in myelinated nerve fibers. The formation and stabilization of channel clusters depends on both cellular and molecular mechanisms. For example, deletion of the cytoskeletal scaffolding protein ankyrinG (AnkG) from axon initial segments results in a failure to cluster Nav channels at these sites (Zhou et al., 1998), and mutant animals with disrupted paranodal attachment of myelin have broadened Nav channel clusters at nodes of Ranvier with reduced densities of channels (Dupree et al., 1999; Boyle et al., 2001; Rasband et al., 2003a; Rios et al., 2003). A variety of other proteins, including AnkG-binding cell adhesion molecules [e.g., neuron–glia related cell adhesion molecule (NrCAM) and Neurofascin-186], are also thought to be important in maintaining and clustering nodal ion channels (for review, see Poliak and Peles, 2003; Salzer, 2003).

The spectrins are a family of submembranous scaffolding proteins that, together with ankyrins, cross-link membrane proteins and actin filaments into a stable and flexible network (Bennett and Baines, 2001). For example, the erythroid spectrins are necessary to maintain the highly deformable and elastic properties of circulating red blood cells. Thus, mutations in erythroid spectrins result in red blood cell membrane instability, spherocytosis, and dysfunction (Marchesi and Steers, 1968; Delaunay, 2002). In contrast, the roles of nonerythroid spectrins are not well understood. Recently, a nonerythroid spectrin, βIV spectrin, was found specifically localized to nodes of Ranvier and AISs and was proposed to link Nav channels to the actin-based cytoskeleton through AnkG (Berghs et al., 2000; Komada and Soriano, 2002). Consistent with this idea, Nav channel clusters in βIV spectrin-null mice are disrupted at nodes and AISs (Komada and Soriano, 2002). Thus, βIV spectrin may be important for nodal membrane structure and the stabilization of Nav channels.

To identify the molecular mechanisms underlying these scaffolding functions of βIV spectrin at nodes of Ranvier, we examined here "quivering" (*qv*) mice with mutations affecting the C-terminal region of βIV spectrin splice variants. A variety of *qv* alleles exist, each with varying degrees of modification to the predicted primary amino acid sequence of βIV spectrins and each showing a phenotype consistent with both sensory and motor neuropathy (Parkinson et al., 2001). We show here that mice with the most conservative mutation (qv^{3J}) have disrupted nodes of Ranvier in the CNS but mostly normal nodes in the PNS. These results indicate that the C-terminal region is required for the nodal retention and stability of βIV spectrins, which are necessary for maintenance of nodal Nav channel clusters and nodal membrane integrity. In addition, these results suggest that additional βIV spectrin-dependent mechanisms exist in the PNS that can attenuate the phenotype resulting from the mutation found in qv^{3J} mutant mice.

Received June 1, 2004; revised June 28, 2004; accepted June 28, 2004.

This work was supported by the National Institutes of Health (M.N.R. and M.S.), a Wadsworth Foundation Young Investigator Award (M.N.R.), the Alexander von Humboldt Foundation (M.S.), and the American Diabetes Association (M.S.). We thank Dr. Peter Shrager for help and the use of his suction electrode equipment to measure CAPs and peak conduction velocities. We thank Dr. James Trimmer for generously providing antibodies and helpful discussions. We thank Dr. Bruce Tempel for generously providing qv^{4J} tissue. We thank Julie Gross and Maya Yankova for technical advice on electron microscopy.

Correspondence should be addressed to Dr. Matthew Rasband, Department of Neuroscience, University of Connecticut Health Center, 263 Farmington Avenue, Farmington, CT 06030-3401. E-mail: rasband@uchc.edu.

DOI:10.1523/JNEUROSCI.2125-04.2004

 0270-6474/04/247230-11$15.00/0

Materials and Methods

βIV spectrin mutant mice. We obtained C57BL/6J-Spnb4^{qv3J}/+ mice from The Jackson Laboratory (Bar Harbor, ME). The mouse line was maintained by heterozygote intercrosses in the animal facility of the University of Connecticut Health Center. The mouse βIV spectrin gene includes 36 exons, and the βIVΣ1 splice variant has a predicted length of 2559 amino acids. The qv^{3J} allele contains a single-base insertion at exon 31 and causes a frame shift at amino acid G2209 (Parkinson et al., 2001). A 551 bp fragment at exon 31 including the site of mutation was amplified by PCR (5′ primer, AGGCAGCGCCTTTGCTGCGTC; 3′ primer, TCCTGGTCACAGAGGTCCTTA). *Sty*I (New England Biolabs, Beverly, MA) was used to distinguish the genotype of the pups. Optic nerve and sciatic nerve tissue from control and qv^{4J} mutant mice was kindly provided by Dr. Bruce Tempel (University of Washington, Seattle, WA).

Gait analysis. The gait analysis method was modified from de Medinaceli et al. (1982) and Ozmen et al. (2002). Mice were tested in a confined walkway 10 cm wide by 30 cm long with a dark shelter at the end. Mice were trained several times to walk into the darkened compartment. After dipping their hindpaws into ink on a sheet of Parafilm, mice walked down the corridor on white paper. The distance between each step or between the first and the fifth toes could be compared on the paw prints.

Antibodies. The anti-Nav channel antibodies used included a pan-specific Nav channel antibody that recognizes all neuronal isoforms (Rasband et al., 1999), a mouse monoclonal anti-Nav1.2, and a polyclonal anti-Nav1.6 (Rasband et al., 2003b). The N-terminal-directed anti-βIV spectrin (anti-βIV NT) antibody was generated against a synthetic peptide corresponding to amino acids 15–38 of the βIVΣ1 splice variant. The following antibodies have been described previously: rabbit polyclonal and mouse monoclonal anti-Kv1.2 antibodies (Rhodes et al., 1995; Bekele-Arcuri et al., 1996), rabbit polyclonal and mouse monoclonal anti-Caspr antibodies (Rasband and Trimmer, 2001; Rasband et al., 2003b), and a rabbit anti-βIV spectrin "specific" domain (SD) antibody (Berghs et al., 2000). The following antibodies were purchased: anti-ErbB2 antibodies (Santa Cruz Biotechnology, Santa Cruz, CA), anti-CNP (2′,3′-cyclic nucleotide 3′-phosphodiesterase), anti-β actin, anti-α tubulin, and anti-medium neurofilament (NF-M; Sigma, St. Louis, MO), anti-light neurofilament (NF-L) and anti-heavy neurofilament (NF-H; Chemicon, Temecula, CA), and anti-ankyrinG (Zymed, San Francisco, CA). Anti-MBP was a gift from Dr. Elisa Barbarese (University of Connecticut Health Center, Farmington, CT) (Barbarese et al., 1977). Polyclonal antibodies were affinity purified and tested for specificity by Western blot and immunofluorescence with and without blocking by a molar excess of the immunizing peptide.

Immunohistochemistry. The immunostaining method is as described previously (Rasband et al., 1999). Briefly, optic nerves and sciatic nerves from *qv* mutant and wild-type (WT) mice were dissected immediately after the animals were killed. Nerves were fixed with ice-cold 4% paraformaldehyde in 0.1 M phosphate buffer (PB), pH 7.2, for 30 min. Nerves were then transferred to ice-cold 20% sucrose solution in 0.1 M PB overnight (in the case of qv^{4J} nerves, the tissue was frozen in 20% sucrose and stored at −80°C). For cryosectioning, nerves were frozen in Tissue-Tek (Miles, Elkhart, IL) OCT mounting medium. Sections were cut in 5-μm-thick (optic nerve) and 10-μm-thick (sciatic nerve) sections, placed in 0.1 M PB, spread on gelatin-coated coverslips, and allowed to air dry. The sections were permeabilized for 1 hr in 0.1 M PB containing 0.3% Triton X-100 and 10% goat serum, pH 7.4 (PBTGS). Sections were incubated overnight with primary antibodies diluted to appropriate concentration in PBTGS. Sections were thoroughly rinsed three times in PBTGS (5 min each), followed by application of fluorescently labeled secondary antibody for 1 hr at room temperature. Secondary antibodies were Alexa 488-conjugated goat anti-mouse/anti-rabbit and Alexa 594-conjugated goat anti-rabbit/anti-mouse antibodies (Molecular Probes, Eugene, OR). Finally, labeled sections were rinsed three times in PBTGS, 0.1 M PB, and 0.05 M PB for 5 min each and mounted on slides. Digital images were collected on a Axioskop 2 (Zeiss, Thornwood, NY) fluorescence microscope fitted with a Hamamatsu (Bridgewater, NJ) ORCA-ER camera. In some instances, a Z-stack of images was collected at 0.2 μm intervals, and the resulting stacks were then deconvolved by iterative restoration using the software package Volocity (Improvision, Lexington, MA). The length of each Nav channel cluster was measured using Openlab software (Improvision).

Immunoblotting. Mouse membrane homogenates were prepared from freshly dissected brains. Each brain was homogenized in ice-cold 0.32 M sucrose, 5 mM sodium phosphate, pH 7.4, and 1 mM sodium fluoride, containing 1 mM phenylmethylsulfonyl fluoride, 2 μg/ml aprotinin, 1 μg/ml leupeptin, 2 μg/ml antipain, and 10 μg/ml benzamidine (10 ml/gm wet brain weight). Crude homogenates were then centrifuged at 600 × *g* for 10 min to remove debris and nuclei. The resulting supernatant was then centrifuged at 45,000 × *g* for 60 min. This pellet was then resuspended in 2.5 ml of ice-cold homogenization buffer per gram of brain used. Protein concentration was determined using the BCA protein assay kit (Pierce, Rockford, IL). Crude brain homogenates were then diluted in reducing sample buffer to a final concentration of 1 μg/μl, and either 20 or 5 μg membrane proteins were loaded and separated by 6–15% SDS-PAGE. Size-fractionated proteins were then transferred to nitrocellulose membranes and probed according to the procedure described previously. Peroxidase-conjugated goat anti-mouse/anti-rabbit IgGs were used for detection with chemiluminescent reagents (PerkinElmer Life Sciences, Wellesley, MA).

Electron microscopy. Three pairs of 3- to 4-month-old [postnatal day 83 (P83), P110, and P125] qv^{3J} mutants and age-matched littermate WT mice were anesthetized with 0.11 ml of sodium pentobarbital by intraperitoneal injection and then perfused with 2% paraformaldehyde and 2% glutaraldehyde in 0.08 M PB, pH 7.4, containing 0.004% calcium chloride. Optic nerves and sciatic nerves were dissected out and postfixed overnight. These nerves were then osmicated, stained, dehydrated, and embedded in Epon. Ultrathin sections (50–70 nm) of both longitudinal and transverse sections were made for poststaining. Electron micrographs were made using a Jeol (Peabody, MA) JEM-100CX electron microscope. Measurements were performed using NIH ImageJ software (available online at http://rsb.info.nih.gov/nih-image/) and Openlab software. Average ± SD values are given.

Electrophysiology. Compound action potentials (CAPs) from six sciatic and six optic nerves from three pairs of WT and qv^{3J} mice (3–5 months old) were recorded using suction electrodes as described previously (Rasband et al., 1999).

Results

Identification and phenotype of qv^{3J} mutant mice

βIV spectrin is a large, alternatively spliced cytoskeletal protein (six βIV spectrin alternative splice variants have been reported: Σ1–Σ4, (Berghs et al., 2000); Σ5, (Tse et al., 2001), and Σ6 (Komada and Soriano, 2002), with diverse protein–protein and protein–lipid interaction domains (Parkinson et al., 2001). To investigate the function of these domains, we chose the qv^{3J} mutant mouse with the most conservative mutation resulting in the smallest change to the predicted primary amino acid sequences of the βIV spectrin splice variants. The qv^{3J} mouse has a single point mutation within the C-terminal SD (Fig. 1*A*, arrowhead) (Berghs et al., 2000; Parkinson et al., 2001); this domain has also been called the "variable region" by other investigators (Komada and Soriano, 2002), resulting in a novel 49 amino acid extension and lacking the pleckstrin homology (PH) domain (Parkinson et al., 2001). Of the reported βIV spectrin splice variants, this mutation is predicted to affect only βIVΣ1, βIVΣ3, and βIVΣ6 (the domain structures of βIVΣ1 and the mutant qv^{3J} βIVΣ1 are shown in Fig. 1*A*).

Because homozygous male qv^{3J} mice are infertile, heterozygous mutants were mated and screened for homozygous qv^{3J} offspring using a PCR-based strategy. Because the *Sty*I restriction enzyme cuts only at the site of the single base pair insertion, it was used to identify mice with the mutant allele(s) (Fig. 1*B*). The genotypes of homozygous qv^{3J} mice (hereafter denoted qv^{3J}) were verified by immunostaining sciatic nerve using antibodies di-

rected against an epitope located in the SD domain of βIV spectrin (anti-βIV SD) (Berghs et al., 2000) distal to the point mutation; anti-βIV SD and anti-Pan Na^+ channel (Pan Nav) immunostaining of sciatic nerve showed that all nodal βIV SD immunoreactivity was lost in qv^{3J} mice (Fig. 1*C*).

Phenotypically, qv^{3J} mice have progressive neurological and motor impairment and a shortened lifespan; the majority of qv^{3J} mice died before 5 months of age. Heterozygous mice are normal; all subsequent experiments reported here were performed using WT and homozygous qv^{3J} mice. When held by the tail, qv^{3J} mice clasp their hindlegs together rather than in a splayed position like control littermates (Fig. 1*D*). Gait analysis of young animals (2–3 months old) at the onset of the overt quivering behavior showed early signs of ataxia, including limb weakness and dragging of the hindlegs (Fig. 1*E*). Older animals (4–5 months) had much more severe ataxia, including paralysis, decreased locomotion, and pronounced quivering (Fig. 1*E*).

Proteins associated with myelinated axons

Because the qv^{3J} phenotype is consistent with demyelinating neuropathy and/or axonal degeneration, WT littermate and qv^{3J} brain membranes were assayed by immunoblot for changes in the amount of proteins associated with myelinated axons or for the specific nodal, paranodal, and juxtaparanodal domains of myelinated axons (Fig. 1*F*). For brain Na^+ channels, there was no difference in the total pool, but the Nav1.2 subtype was slightly increased in qv^{3J} mice. In contrast, the amount of Caspr (a paranodal protein) (Peles et al., 1997) was reduced in qv^{3J} animals compared with WT, but the levels of Kv1.2 (a juxtaparanodal protein) (Wang et al., 1993) were unchanged. Immunoblotting with antibodies against the myelin proteins MBP and CNP showed no significant differences. The cytoskeletal proteins β-actin and α-tubulin were also unchanged. As expected (Berghs et al., 2000), immunoblots using anti-βIV SD antibodies showed two proteins of ~250 and ~140 kDa corresponding to βIVΣ1 and βIVΣ6 spectrins, respectively, but the lane containing qv^{3J} brain membranes had no immunoreactivity. Although Nav1.2 is typically associated with unmyelinated axons (Gong et al., 1999; Boiko et al., 2001), it has been shown to be increased in animals with inflammatory and genetic hypomyelination or demyelination (Westenbroek et al., 1992; Craner et al., 2003; Rasband et al., 2003b). The reduction in Caspr could be related to a loss of paranodal structures and has been suggested as an early indicator of demyelination (Salzer, 2003).

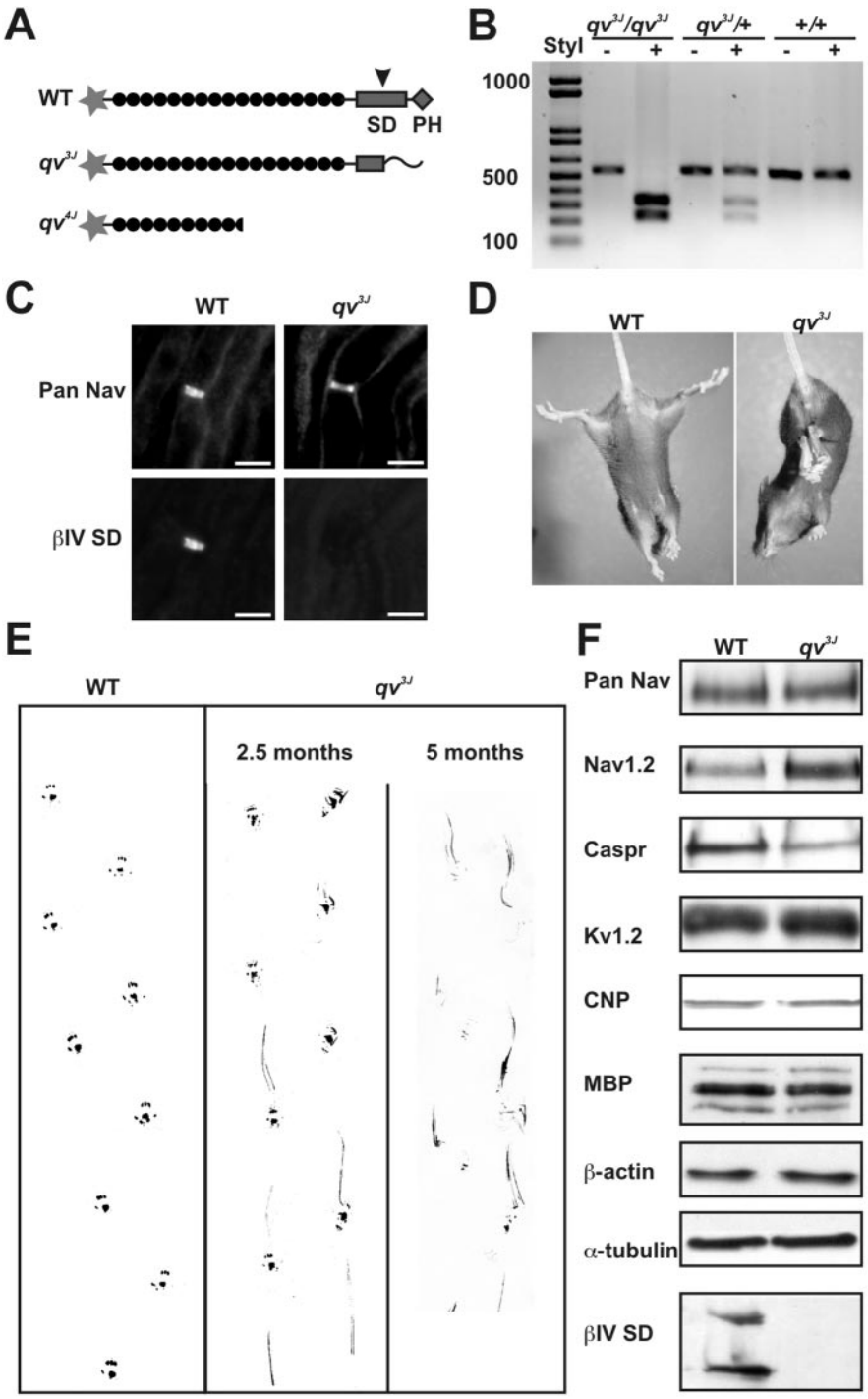

Figure 1. Identification and phenotype of qv^{3J} mice. *A*, Schematic of WT, qv^{3J}, and qv^{4J} mutant βIV spectrin. *B*, PCR-based screening for qv^{3J} homozygous mutant mice using the *StyI* restriction enzyme. *C*, Double immunostaining of rat sciatic nerve with antibodies against Nav channels (Pan Nav) or the SD domain of βIV spectrin (βIV SD) shows that the βIV SD epitope is absent in qv^{3J} mice. *D*, *E*, qv^{3J} mice clasp their hindlegs together and have significant gait abnormalities, including weakness, tremor, and a dragging of their hindlegs. *F*, Immunoblot analysis for a variety of proteins associated with myelinated axons, including Nav channels (Pan Nav, Nav1.2), Caspr, Kv1.2, CNP, MBP, β-actin, α-tubulin, and SD-containing βIV spectrin isoforms. Scale bars, 5 μm.

qv^{3J} mice have aberrant CNS nodes of Ranvier

Myelination and the various axolemmal domains were examined by immunofluorescence (Fig. 2) and electron microscopy (Fig. 3) to determine whether the qv^{3J} mutation results in dysmyelination, altered node of Ranvier formation, and/or axonal degeneration. Immunostaining of 3-month-old qv^{3J} optic nerves with

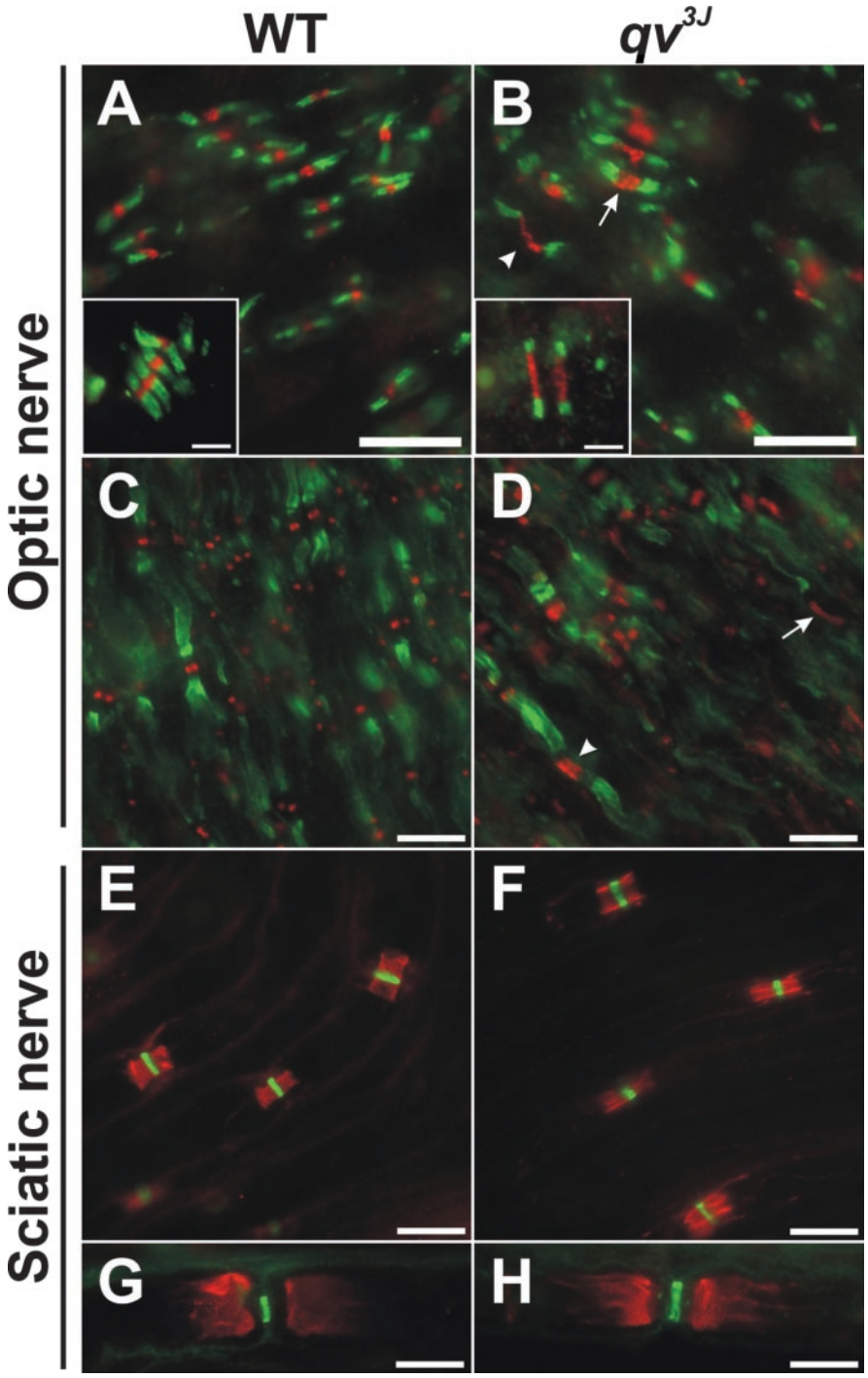

Figure 2. Nodal Nav channel clusters are disrupted in the CNS of qv^{3J} mutants, but PNS nodes are normal. *A*, *B*, Double immunostaining for Nav1.6 (red) and Caspr (green). Nav1.6 clusters were often broader in qv^{3J} mutant mice (*B*, *D*, arrow and inset). *C*, *D*, Double immunostaining for Kv1.2 (green) and Nav1.6 (red). *E*, *F*, Double immunostaining for Caspr (red) and Nav1.6 (green). *G*, *H*, Kv1.2 (red) and Nav1.6 (green) immunostaining. Scale bars: *A–H*, 10 μM; insets, 2 μM.

antibodies against Caspr (green) and Nav1.6 (red), the main adult nodal Nav channel (Caldwell et al., 2000; Boiko et al., 2001), showed that many Nav1.6-labeled qv^{3J} nodes were longer than WT nodes (Fig. 2, compare *A*, arrowhead and *B*, inset). Nodal Nav1.6 clusters in qv^{3J} mice were on average twice the length of WT clusters and were significantly wider (Table 1). When Nav1.6 channel clusters were increased in length, the immunoreactivity appeared granular and less intense (Fig. 2*B*, arrow and inset, and *D*, arrow). In addition, paranodal Caspr staining was often substantially shorter in length (Fig. 2*B*, inset). Although immunoblot analysis of brain membranes showed an increase in Nav1.2 protein, we did not detect Nav1.2 at optic nerve nodes in qv^{3J} mice (data not shown). In both WT and qv^{3J} mutant mice, Kv1.2 immunoreactivity (green) usually appeared in the juxtaparanode (Fig. 2*C*,*D*). In a few instances in which Nav1.6 staining (red) was present in elongated clusters, Kv1.2 immunoreactivity extended to the node without a paranodal gap (data not shown).

In the peripheral nervous system, immunostaining of qv^{3J} sciatic nerve nodes of Ranvier for nodal Nav1.6 (green) and paranodal Caspr (red) (Fig. 2, compare *E*, *F*), or Nav channels (green) and juxtaparanodal Kv1.2 (red) (Fig. 2, compare *G*, *H*) showed no significant change in the localization of these proteins. Occasionally (much less than 1% of nodes), Kv1 channels were detected in nodal regions (similar to what we observed frequently in other *qv* mutants; see below). No difference in the length or width of nodal Nav1.6 clusters was detected by immunofluorescence (Table 1).

Electron microscopic analysis of longitudinal optic nerve sections showed a similar increase in node length in qv^{3J} mice (Table 1; Fig. 3, compare *A*, WT and *B*, qv^{3J}; arrows delineate the nodal gap). Close examination of paranodal structures revealed that axoglial junctions were normal; all loops directly apposed the axolemma and transverse bands were clearly detected (Fig. 3*C*, arrows). However, 52% ($n = 79$) of qv^{3J} nodes had striking membrane protrusions (Fig. 3*D*, arrows delineate the ends of paranodes). These structures were often filled with vesicles, debris, and mitochondria. Similar protrusions were not seen in the optic nerves of WT mice.

In contrast to the CNS, electron microscopic analysis of PNS nodes of Ranvier confirmed that there was no difference in the length of WT and qv^{3J} nodes (Table 1). Longitudinal sections showed that the majority of qv^{3J} nodes had no significant ultrastructural changes, but 5 of 19 (26%) qv^{3J} peripheral nodes showed some degree of nodal membrane protrusion (Fig. 3, compare *E*, WT and *F*, qv^{3J}, arrow). In both WT and mutant qv^{3J} mice, the nodal gap was filled with Schwann cell microvilli. Similarly, cross sections through nodes showed that microvilli were still in contact with the nodal membrane and appeared unchanged. However, the nodal axolemma appeared irregular in qv^{3J} mice, and, in some cases, there appeared to be an accumulation of vesicles (Fig. 3, compare *G*, WT and *H*, qv^{3J}, arrow). Together, these results suggest that the SD and PH domains are critical for βIV spectrin function and/or stability and ultimately

for the integrity of nodal membrane structure. In addition, the effects of the qv^{3J} mutation appeared to be more dramatic in the CNS than PNS, suggesting that additional mechanisms exist in the PNS that can attenuate the consequences of βIV spectrins lacking the SD and PH domains.

Axon shape and cytoskeletal organization are altered in qv^{3J} mice

Cross sections of optic nerves and sciatic nerves showed that, as for WT mice, myelin was appropriately compacted in the qv^{3J} mutant (Fig. 4, compare *A*, WT and *B*, qv^{3J}; sciatic nerve not shown). However, myelinated qv^{3J} optic nerve axons were highly convoluted compared with the normal, more cylindrical shape (Fig. 4 *B*, *D*, inset); cross sections of qv^{3J} sciatic nerves showed no significant difference in shape (data not shown). To quantify the difference in shape between optic nerve axons in WT and qv^{3J} mice, we calculated a shape factor of S for each axon [$S = 4 \times \pi \times \text{area}/(\text{perimeter})^2$; S is close to 1 for nearly cylindrical axons, whereas more irregularly shaped axons have values <1]. The qv^{3J} axons were significantly less cylindrical than WT axons (Table 1). The change in shape was even more dramatic for larger fibers (>2 μm^2) than for small fibers (Table 1). Finally, we did not observe any axonal degeneration in the optic nerve. These results suggest that βIV spectrin is important not only for nodes but also for membrane shape and structure throughout the axon.

A close examination of the cytoskeleton in longitudinal and cross sections of optic nerve showed that qv^{3J} axons had a large increase in filamentous material compared with WT mice (Fig. 4, compare *C*, WT and *D*, qv^{3J}). Higher magnification showed that there was an increase in neurofilament density rather than in microtubule density (Fig. 4, compare *E*, *F*, arrows). Immunoblot analysis showed no change in the levels of either actin or tubulin (Figs. 1*F*, 4*G*) or in NF-L and NF-H (Fig. 4*G*). However, NF-M was significantly increased. Thus, the qv^{3J} mutation in βIV spectrin results in widespread cytoskeletal changes in the axons of the optic nerve.

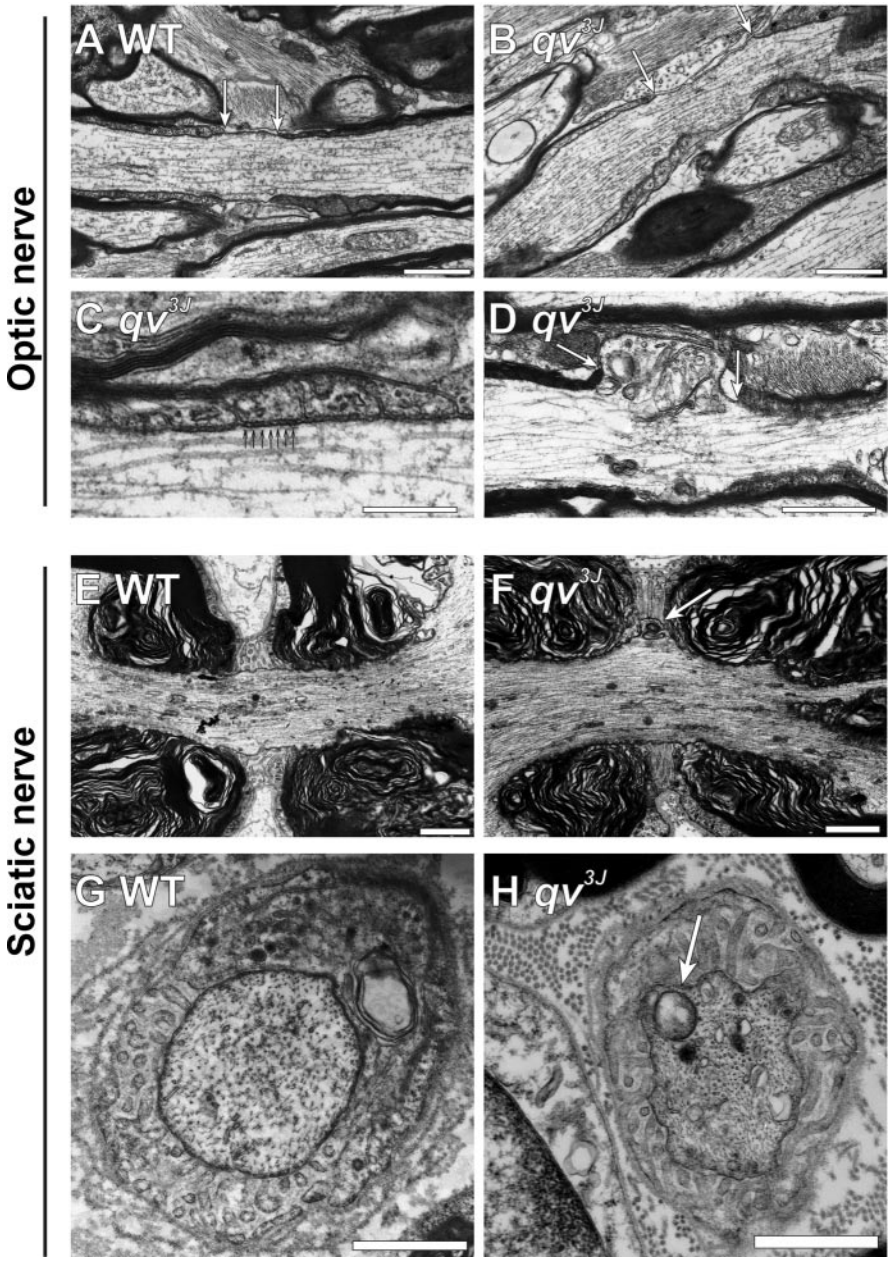

Figure 3. Node length and nodal membrane shape are distorted in qv^{3J} mutant mice. *A*, WT node of Ranvier from 4-month-old optic nerve. *B–D*, Optic nerve nodes of Ranvier from 4-month-old qv^{3J} mice are significantly longer (*B*). Paranodes in qv^{3J} mice have transverse bands (*C*, arrows). Many CNS nodes of Ranvier from qv^{3J} mice have prominent nodal protrusions. Arrows delineate the edges of the myelin sheath in *A*, *B* and *D*, *E*. *F*, Longitudinal sections of sciatic nerve nodes of Ranvier from 4-month-old WT and qv^{3J} mice. Occasionally, nodal protrusions and vesicles were observed in qv^{3J} mice (*F*, arrow). *G*, *H*, Cross sections through sciatic nerve nodes of Ranvier from WT (*G*) and qv^{3J} (*H*) mice. Note that, although the membrane is deformed and there is an increase in vesicles in the axon in the qv^{3J} mutant, the Schwann cell microvilli are normal in appearance. Scale bars: *A–F*, 1 μm; *G*, *H*, 2 μm.

AnkyrinG and mutant βIV spectrin can be detected at nodes in qv^{3J} mice

Double immunostaining using βIV NT and Pan Nav antibodies showed that these proteins colocalized in WT optic nerves (Fig. 5*A*, *A′*), but βIV NT immunoreactivity was absent in qv^{3J} optic nerves (Fig. 5*C*, *C′*; *C′* shows a single broad Nav channel cluster). Immunoreactivity for AnkG, an adapter protein thought to link Nav1.6 to βIV spectrin, colocalized with Nav1.6 in mutant qv^{3J} optic nerves (Fig. 5, compare *B*, *B′*, WT and *D*, *D′*, qv^{3J}, arrows). However, the staining intensity of AnkG was reduced and distributed in broader clusters in the qv^{3J} mutant. Thus, although AnkG was detected at CNS nodes, βIV spectrin was not.

In the PNS, βIV spectrin and AnkG immunoreactivities colocalized with Pan Nav staining and were detected at every node of Ranvier in the WT sciatic nerve (Fig. 5*E*, *E′*, *F*, *F′*). However, the immunostaining for these proteins was significantly attenuated in qv^{3J} mice (Fig. 5*G*, *G′*, arrows, and *H*, *H′*). Whereas WT nodes had βIV spectrin immunoreactivity that was confined between Caspr-labeled paranodes (Fig. 5*I*, *I′*), 60% (30 of 51) of qv^{3J} nodes had no detectable

Table 1. Node length, peak conduction velocity, and radius of axonal curvature measured for WT and qv^{3J} mutant mouse fibers

	EM node length (μm)	IF node length (μm)	IF node width (μm)	Conduction velocity 37°C (m/sec)	Conduction velocity 25°C (m/sec)	Radius of curvature	Radius of curvature axons >2.0 μm²
Optic nerve							
WT	0.82 ± 0.18	1.03 ± 0.30	1.04 ± 0.29	7.18 ± 1.13	3.84 ± 0.77	0.81 ± 0.26	0.83 ± 0.13
	($n = 53$)	($n = 108$)	($n = 100$)	($n = 6$)	($n = 6$)	($n = 300$)	($n = 18$)
qv^{3J}	1.63 ± 0.70	2.08 ± 0.78	1.26 ± 0.40	8.47 ± 1.54	4.37 ± 1.06	0.60 ± 0.23	0.34 ± 0.11
	($n = 79; p < 0.001$)	($n = 175; p < 0.001$)	($n = 100; p < 0.0001$)	($n = 6; p = 0.13$)	($n = 6; p = 0.34$)	($n = 300; p < 0.001$)	($n = 16; p < 0.001$)
Sciatic nerve							
WT	1.19 ± 0.22	1.16 ± 0.15	2.52 ± 1.00	63.3 ± 21	41.7 ± 5.2		
	($n = 12$)	($n = 45$)	($n = 100$)	($n = 6$)	($n = 6$)		
qv^{3J}	1.39 ± 0.33	1.17 ± 0.19	2.79 ± 1.17	56.0 ± 24.5	38.2 ± 9.3		
	($n = 17; p = 0.08$)	($n = 59; p = 0.79$)	($n = 100; p = 0.08$)	($n = 6; p = 0.59$)	($n = 6; p = 0.45$)		

EM, Electron microscopy; IF, immunofluorescence. Errors are given as mean ± SD.

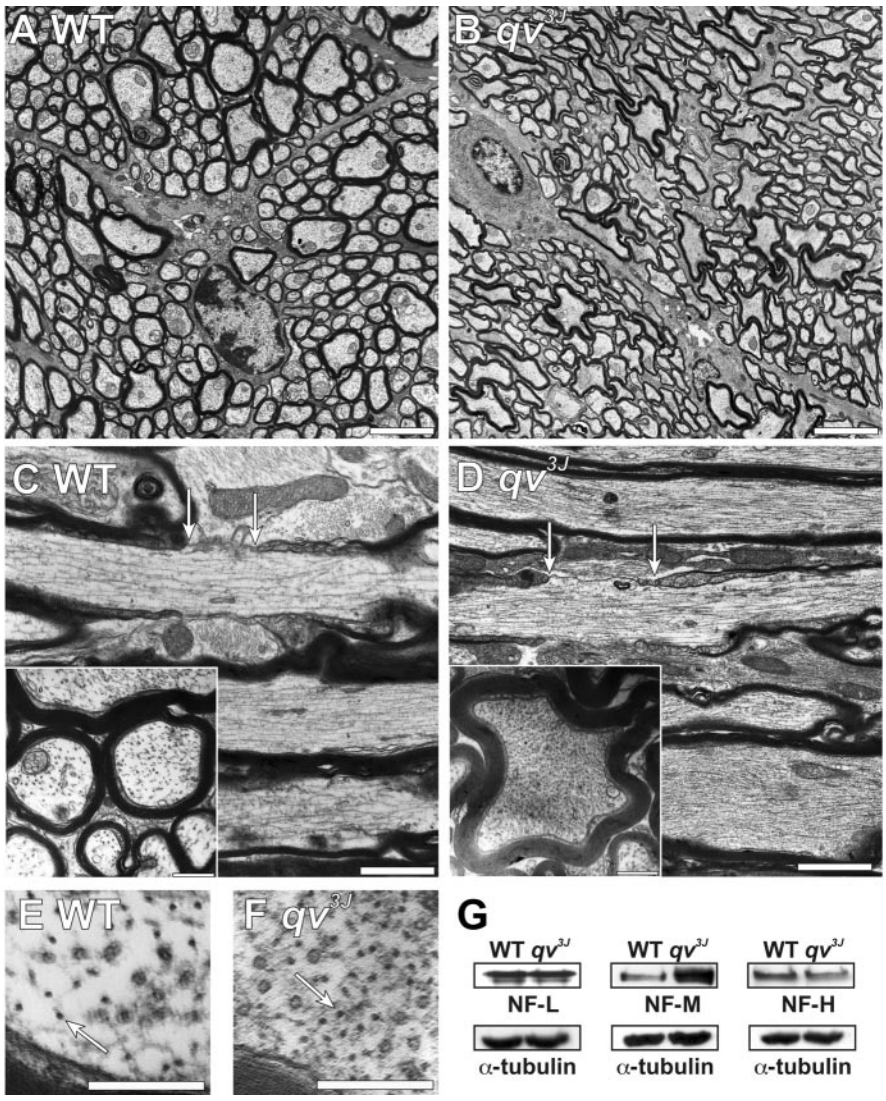

Figure 4. Four-month-old qv^{3J} mice have dramatic changes in axon shape and cytoskeletal organization. *A*, *B*, Transverse optic nerve sections from WT (*A*) and qv^{3J} (*B*) mice show that qv^{3J} mouse axons are highly convoluted and not cylindrical. *C*, *D*, Longitudinal and transverse (inset) cross sections show that, compared with WT mice (*C*), qv^{3J} mice have a dramatic increase in the density of cytoskeletal elements (*D*). Nodes of Ranvier are delineated by arrows. *E*, *F*, High magnification of optic nerve cross sections shows qv^{3J} mice (*F*, arrow) have an increased density of neurofilaments compared with WT mice (*E*). *G*, Immunoblotting for neurofilament proteins shows that, in contrast to NF-L and NF-H, the amount of NF-M is increased in qv^{3J} mutant mice. The same blots were probed for α-tubulin as a control for protein loading. Scale bars: *A*, *B*, 3 μm; *C*, *D*, 1 μm; inset, 0.5 μm; *E*, *F*, 0.25 μm.

βIV NT immu-noreactivity (Fig. 5*J*,*J*′), 40% of qv^{3J} nodes had some weak βIV NT staining (Fig. 5*K*,*K*′), and, in one isolated instance, βIV NT immunostaining in qv^{3J} mice was nearly as intense as that seen in WT mice (Fig. 6*L*,*L*′). Importantly, qv^{3J} mouse retinal ganglion cells and cerebellar Purkinje cells did not have βIV spectrin that had accumulated in cell bodies (data not shown). Together, these results suggest that βIV spectrin protein can traffic appropriately to nodes of Ranvier, but, in the absence of the SD and PH domains, it fails to be retained at these sites and may be more rapidly destroyed.

Compound action potentials are mostly normal in qv^{3J} mice

CAPs recorded from sciatic nerves isolated from 3- to 5-month-old WT and qv^{3J} mice showed that the shape of the CAP (Fig. 6*A*), the calculated peak conduction velocities (Fig. 6*B*) ($n = 6$), and the absolute refractory periods (data not shown) were not significantly different at either 25°C or 37°C. These results are not surprising given the lack of changes in ion channel localization and clustering in the qv^{3J} PNS. However, despite dramatic changes at nodes of Ranvier in the CNS, the amplitudes and shape of optic nerve CAPs from qv^{3J} mice were only slightly different from WT mice (Fig. 6*A*). In some recordings, the second peak of the optic nerve CAP was larger in qv^{3J} optic nerves. This second, slower peak may be attributable to more fibers conducting action potentials at a slower velocity. However, because optic nerve CAPs result from the sum of many thousands of individual action potentials, it is difficult to draw definitive conclusions from changes in amplitudes. Furthermore, the peak optic nerve conduction velocities (calculated from the

time to the first peak of the CAP) showed no significant differences ($n = 6$) (Fig. 6*B*). Thus, the quivering phenotype may be related to decreased conduction velocities in the CNS. Alternatively, reduced densities of Nav channels at axon initial segments may account for the qv^{3J} phenotype. Consistent with the latter idea, Nav1.6 immunofluorescence staining is reduced at qv^{3J} axon initial segments (Fig. 5*M*,*N*, arrowheads).

Loss of the ankyrinG binding domain disrupts PNS nodes of Ranvier

To determine whether the phenotype observed in the qv^{3J} mouse was a specific consequence of the truncation and loss of the SD and PH domains, respectively, we examined nodes of Ranvier in another *qv* mutant mouse harboring the qv^{4J} allele (Parkinson et al., 2001). These mice have a point mutation that results in a premature stop codon in the 10th spectrin repeat. As a consequence, the reported βIV spectrin splice variants βIVΣ1, βIVΣ3, and βIVΣ6 are predicted to be 60, 8, and 3% of normal length, respectively. The qv^{4J} mutation deletes the AnkG binding domain (Komada and Soriano, 2002). As with qv^{3J} mice, qv^{4J} mice are ataxic, have a reduced lifespan, exhibit deafness (Parkinson et al., 2001), and have disrupted CNS nodes of Ranvier (data not shown). In contrast to qv^{3J} PNS nodes of Ranvier, which appeared normal by light microscopy (Fig. 2*F*,*H*), qv^{4J} PNS had a dramatic reorganization in the localization of nodal, paranodal, and juxtaparanodal proteins. Whereas WT mice had nodal Nav channels (red) flanked on each side by paranodal Caspr (green) (Fig. 7*A*) or juxtaparanodal Kv1.2 K^+ channels (green) (Fig. 7*C*), qv^{4J} mice had many disrupted and apparently degenerating nodes of Ranvier with prominent Nav channel immunoreactivity along the axon and disrupted paranodal junctions (Fig. 7*B*, arrow). Normal appearing nodes of Ranvier with clustered Nav channels flanked by Caspr were also present (Fig. 7*B*, arrowhead). Importantly, immunostaining using anti-Caspr (red) and βIV NT antibodies (green) showed that truncated βIV spectrin was undetectable at qv^{4J} nodes (Fig. 7*A*, inset, WT and *B*, inset, qv^{4J}), consistent with the previously reported reduction in levels of βIV spectrin mRNA in these mutant mice (Parkinson et al., 2001). Normal appearing nodes often had aberrant Kv1.2 immunostaining that overlapped with Nav channels and extended into outer paranodal zones (Fig. 7*D*, arrows, overlap is yellow). In contrast to other mutant mice with disrupted paranodes (e.g., Caspr-null and contactin-null) (Bhat et al., 2001; Boyle et al., 2001), Kv1.2 did not extend all the way through the paranode, suggesting that it is only the outermost axoglial junctions that are disrupted and that Kv1.2 targeting to specific domains is altered.

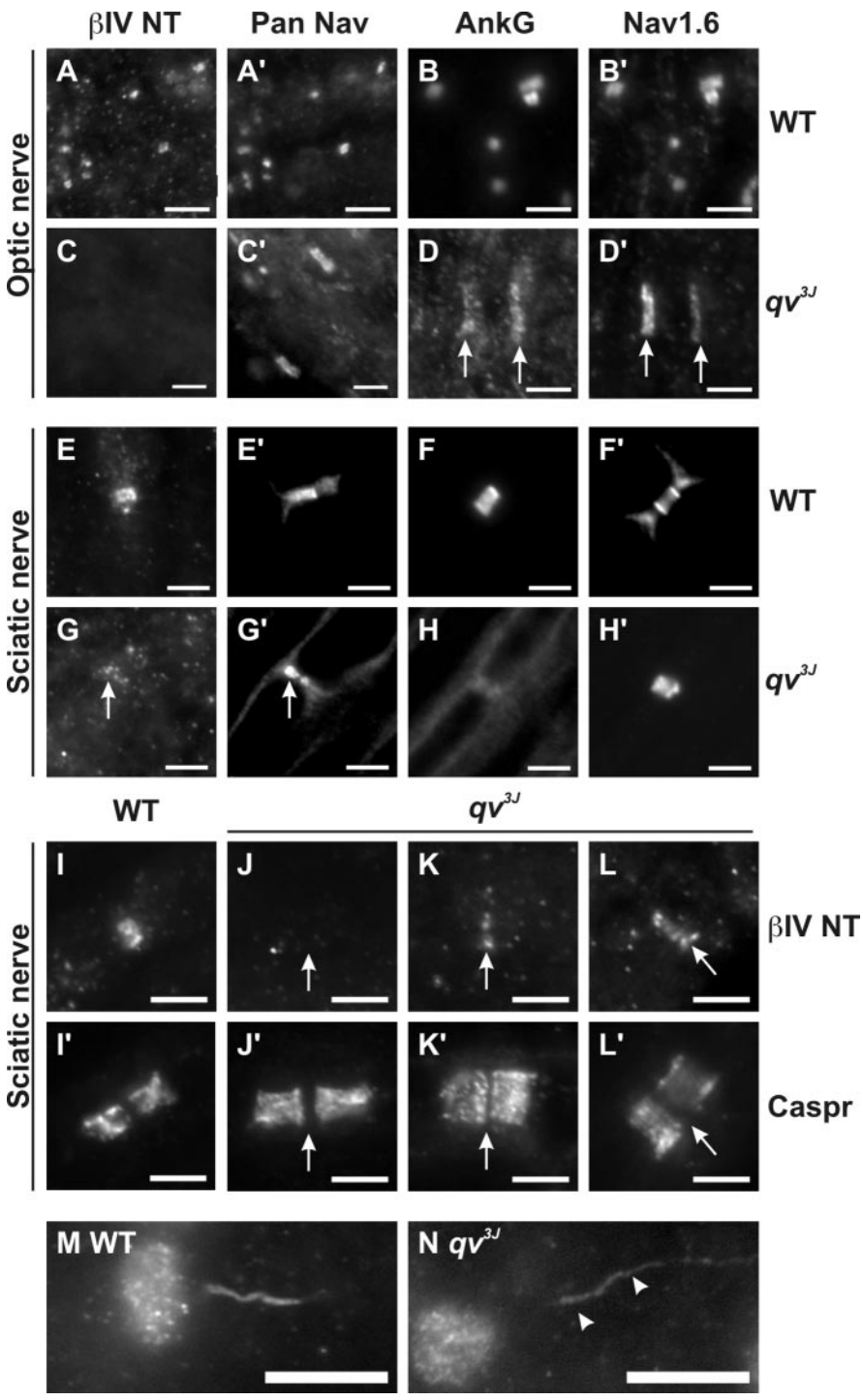

Figure 5. Trafficking of βIV spectrin is not altered in qv^{3J} mice. Double labeling of WT or qv^{3J} optic (*A–D*) and sciatic (*E–H*) nerves using βIV NT (N-terminal; *A*, *C*, *E*, *G*) and Pan Nav (*A′*, *C′*, *E′*, *G′*) or AnkG (*B*, *D*, *F*, *H*) and Nav1.6 (*B′*, *D′*, *F′*, *H′*) antibodies. Double immunostaining of WT (*I*, *I′*) and qv^{3J} (*J–L*) sciatic nerve nodes of Ranvier with βIV NT (*I–L*) and anti-Caspr antibodies (*I′*, *J′*, *K′*, *L′*). In qv^{3J} optic nerve, βIV NT immunoreactivity is undetectable. However, in the qv^{3J} PNS, βIV NT was detected in reduced amounts at ~40% of nodes (*G*, *K*, *L*). AnkyrinG immunoreactivity was detectable in qv^{3J} nodes but reduced in amount and in broader clusters in the CNS (*D*, arrows). Compared with WT mouse initial segments (*M*), Nav 1.6 immunoreactivity was reduced at axon initial segments in qv3J mutant mice (*N*). Scale bars: *A–H*, 3 μm; *I–L*, 5 μm; *M*, *N*, 10 μm.

Double immunostaining nodes of Ranvier with Pan Nav (red) and ErbB2 antibodies (green), the latter having been described

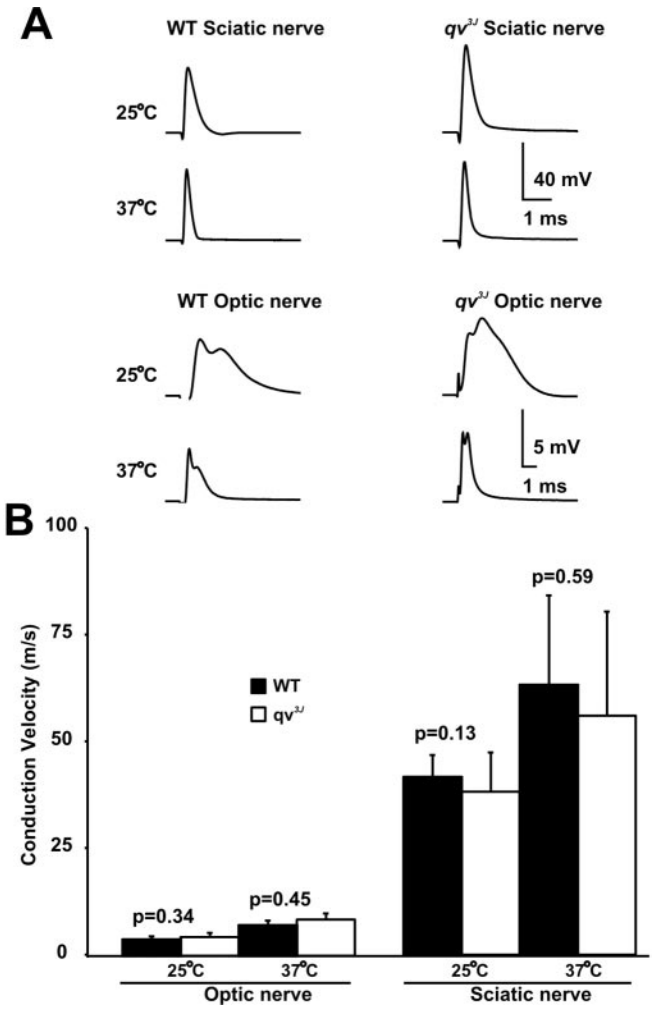

Figure 6. Compound action potentials from PNS and CNS nerves in qv^{3J} mice. *A*, Examples of CAPs recorded from WT and qv^{3J} sciatic and optic nerves at 25°C and 37°C. CAPs were recorded using suction electrodes. *B*, Peak conduction velocities. Error bars indicate ±SD.

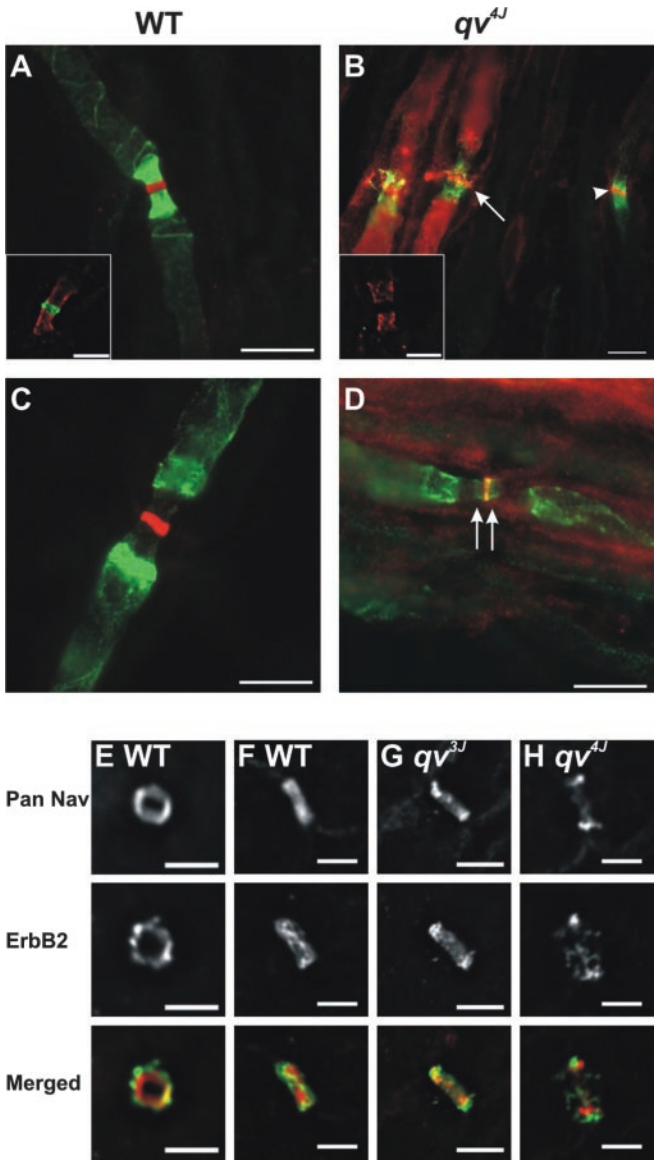

Figure 7. Nodes of Ranvier are disrupted in the PNS of qv^{4J} mutant mice. *A*, *B*, Immunostaining for Caspr (green) and Pan Nav channels (red) shows qv^{4J} mice have many disrupted nodes (*B*, arrow). *C*, *D*, Double labeling for Pan Nav channels (red) and Kv1.2 (green) shows Kv1 channels invade into nodal regions in the qv^{4J} mutant mouse (arrows). *E–H*, Double labeling with Pan Nav (red) and anti-ErbB2 (green) antibodies shows that, compared with WT (*E*, *F*) and qv^{3J} mice (*G*), Schwann cell microvilli in qv^{4J} mice (*H*) are disrupted. Note that, in *F–H*, axons run diagonally from bottom left corner to top right corner. Scale bars: *A–D*, *F–H*, 5 μm; *E*, 3 μm.

previously in Schwann cell microvilli (Kim et al., 2002), showed that ErbB2 immunoreactivity was present in a well defined and compact halo around Nav channels in WT mice (Fig. 7*E*,*F*). Importantly, qv^{3J} mice also had focal ErbB2 immunoreactivity that surrounded the node of Ranvier (Fig. 7*G*). In contrast, ErbB2 immunoreactivity in qv^{4J} mice appeared disrupted, was more diffuse, and did not overlap completely with Nav channels (Fig. 7*H*). These results suggest that the loss of the SD and PH domains may not totally preclude βIV spectrin function and stability, whereas a larger truncation of βIV spectrin, like that found in qv^{4J} mice, is sufficient to disrupt peripheral nodes and Schwann cell microvilli.

Discussion

The clustering and retention of membrane proteins at nodes of Ranvier is essential for action potential conduction. The mechanisms responsible for this are only now being discovered. For example, several nodal ion channels and cell adhesion molecules, including Nav1.6, Kv3.1b, KCNQ2, NrCAM, and Neurofascin-186, may be clustered at nodes, in part, through their interaction with AnkG (Lambert et al., 1997; Devaux et al., 2003, 2004; Lemaillet et al., 2003). Some studies have suggested that AnkG may be one of the first proteins at nascent nodes, even before Nav channels (Rasband et al., 1999; Jenkins and Bennett, 2002). Furthermore, at the AISs AnkG may coordinate assembly of many of the same proteins present at nodes of Ranvier (Jenkins and Bennett, 2001). These observations suggest that interactions between the cytoskeleton and AnkG may be important for node of Ranvier formation and maintenance. This hypothesis can now be tested because βIV spectrin has been identified as the link between AnkG and the axonal cytoskeleton (Berghs et al., 2000; Komada and Soriano, 2002). Recently, Komada and Soriano (2002) showed that βIV spectrin-deficient mice have reduced densities of Nav channels at both PNS nodes and CNS AISs. In the results described here, we show that, in addition to regulating the levels of nodal Nav channels through AnkG, βIV spectrin also functions to maintain nodal membrane integrity and axon shape in myelinated nerve fibers. Furthermore, by using the qv^{3J} mutant

mouse, we show that these properties depend on the C terminus of βIV spectrin, including the SD and PH domains.

The SD and PH domains of βIV spectrin

How does the qv^{3J} mutation disrupt nodes? Truncation of the SD domain and deletion of the PH domain appear not to affect trafficking of the protein but rather its stability and nodal retention. Although the role of the SD domain remains unknown, it is proline rich and may be important for protein–protein interactions. In contrast, PH domains participate in cytoskeleton–plasma membrane adhesion and membrane polarization through their binding to phosphorylated phosphoinositides (Lemmon et al., 2002). One of the most prominent features of the qv^{3J} mutant is the increased node length and the frequent nodal membrane protrusions observed at CNS and PNS nodes. These abnormalities are consistent with a role for βIV spectrin in maintaining nodal membrane structure. βIV spectrin may provide a molecular scaffold not only for proteins but also for the appropriate lipid composition and quantity. Interestingly, a recent study by Nakada et al. (2003) showed that the diffusion of lipids in the AIS membrane was limited. Because the molecular organization of the axon initial segment is similar to the node of Ranvier in many respects (Jenkins and Bennett, 2001), the limited diffusion of phospholipids may be related to their interaction with the PH domain of βIV spectrin. In the absence of βIV spectrin binding to phosphoinositides in the qv^{3J} mutant, the lipid composition may become perturbed, and channels and lipids may be more labile and the overall membrane structure disrupted. Thus, Nav channel retention and membrane stability at nodes of Ranvier may depend not only on protein–protein interactions but also protein–lipid interactions. Based on the observation that Kv1.2 was detected at some disrupted nodes in the qv mutants, we speculate that this regulation may extend even to the kinds of proteins that can partition into the nodal membrane, allowing for the lipid composition to influence the kinds of proteins that can be excluded from or found in the node. Consistent with this idea, Schafer et al. (2004) showed recently that paranodal regions of myelinated fibers have lipid raft-like properties.

Node of Ranvier stability in the PNS

Why is the qv^{3J} mutation more severe in the CNS? The simplest explanation is that nodal integrity is a function of the amount of βIV spectrin that is retained at the node. This conclusion is consistent with the fact that truncated βIV spectrin was undetectable in the CNS of qv^{3J} mice, but low levels of the protein were present at 40% of PNS nodes. Furthermore, βIV NT immunoreactivity was undetectable at PNS nodes of the more severely affected qv^{4J} mice. These observations may reflect slower turnover rates of βIV spectrins in the qv^{3J} PNS compared with the CNS. However, antibody sensitivity combined with different concentrations of spectrins may also underlie the inability to detect diminished levels of βIV spectrin at the CNS node compared with PNS nodes.

Alternatively, a major difference between CNS and PNS nodes is the presence of Schwann cell microvilli. Careful examination of qv^{3J} PNS nodes showed that these structures are normal. A variety of proteins have been described in microvilli (Trapp et al., 1989; Melendez-Vasquez et al., 2001; Scherer et al., 2001; Kim et al., 2002; Goutebroze et al., 2003). Recent experiments in culture have suggested that many of these proteins accumulate at the tips of Schwann cells during early myelination and that microvilli may be involved in Nav channel clustering (Melendez-Vasquez et al., 2001; Gatto et al., 2003). In support of the latter idea, Saito et al. (2003) deleted Schwann cell dystroglycan and found that this results in disrupted microvilli and reduced densities of Nav channels at nodes of Ranvier. Together, these experiments point to a model wherein microvilli are important for the formation of nodes of Ranvier (Salzer, 2003). The analyses of qv^{3J} and qv^{4J} mutant mice are significant because they suggest that microvilli are important not only for node formation but may also contribute to maintenance of mature nodes. With the reduced densities of axonal components like βIV spectrin, it is possible that microvilli can partially compensate by stabilizing the nodal axolemma through as yet unidentified molecular mechanisms. However, when βIV spectrin cannot be detected at nodes, as in the qv^{4J} mice, Schwann cell microvilli are unable to overcome the deficit.

Why are nodes in the PNS of qv^{4J} mutants more disrupted than in qv^{3J} mice? βIV spectrin is alternatively spliced, with six reported variants: Σ1–Σ4 (Berghs et al., 2000), Σ5 (Tse et al., 2001), and Σ6 (Komada and Soriano, 2002). Berghs et al. (2000) showed previously that βIV SD immunoreactivity colocalizes precisely with Pan Nav and AnkG immunostaining in peripheral and central nodes of Ranvier, suggesting that βIVΣ1, βIVΣ3, and/or βIVΣ6 may be present at nodes, because each of these splice variants has the SD epitope. However, other data suggested that βIVΣ1 and a 140 kDa βIV spectrin (Berghs et al., 2000), likely βIVΣ6 (Komada and Soriano, 2002), are the major βIV spectrin splice variants expressed in the nervous system. Our results indicate that at least the βIVΣ1 splice variant is present at nodes of Ranvier of qv^{3J} mice, because nodes are also immunolabeled by βIV NT antibodies (Fig. 5*A*,*E*). However, we cannot rule out βIVΣ6 because these two splice variants cannot be distinguished by immunostaining. The qv^{4J} mutation is predicted to result in βIVΣ1 and βIVΣ6 proteins that are 60 and 3% of normal length, respectively. It is possible that both splice variants are important for nodes and the nearly complete deletion of βIVΣ6 accounts for the more disrupted PNS nodes observed in the qv^{4J} mutant.

A major difference between the qv^{3J} mutation and the qv^{4J} mutation is that the AnkG binding domain is deleted in the qv^{4J} mutant. βIV spectrin may be retained at nodes through the action of both AnkG binding and SD–PH domains. Deletion of both may destabilize spectrins, and thereby the nodes, beyond that which occurs with loss of the PH and SD domains alone. Consistent with this idea, βIV NT immunoreactivity can still be found at some peripheral nodes in qv^{3J} mice but not in the qv^{4J} mutant.

Regulation of neurofilament density by βIV spectrin

An unexpected result from the analysis of the qv^{3J} mutant was a dramatic increase in neurofilament density, an increase in NF-M, and the convoluted shapes of the fibers. Previous studies have shown that axonal diameter is regulated by neurofilament packing (de Waegh et al., 1992; Elder et al., 1999) and that NF-M is the key neurofilament subunit regulating radial axon outgrowth (Garcia et al., 2003; Rao et al., 2003). Although βIV spectrin is thought to be restricted mainly to nodes of Ranvier and axon initial segments in neurons, the results presented here show that the loss of βIV spectrin from nodes can influence the shapes of myelinated axons and the amount of NF-M. Interestingly, in normal PNS axons, there is a reduction in the density of neurofilaments at nodes of Ranvier (Berthold, 1978). Because βIV spectrin is highly enriched at nodes, it is easy to speculate that this protein may act as a negative regulator of NF-M subunits and control neurofilament density. Alternatively, βIV spectrin may be found throughout the axon at levels undetectable by immunofluorescence microscopy, and this non-nodal βIV spectrin may contrib-

ute to neurofilament density and overall axon shape. Finally, we cannot rule out the possibility that the qv^{3J} mutation results in a gain of function that increases neurofilament density and expression levels and that the nodal defect is secondary to the disruption of this neurofilament organization.

In summary, the results reported here suggest that both protein–protein and protein–lipid interactions between βIV spectrin, AnkG (and its associated membrane proteins), and the plasma membrane are required for proper cytoskeletal organization and node of Ranvier formation, function, and stability.

References

Barbarese E, Braun PE, Carson JH (1977) Identification of prelarge and presmall basic proteins in mouse myelin and their structural relationship to large and small basic proteins. Proc Natl Acad Sci USA 74:3360–3364.

Bekele-Arcuri Z, Matos MF, Manganas L, Strassle BW, Monaghan MM, Rhodes KJ, Trimmer JS (1996) Generation and characterization of subtype-specific monoclonal antibodies to K^+ channel alpha- and beta-subunit polypeptides. Neuropharmacology 35:851–865.

Bennett V, Baines AJ (2001) Spectrin and ankyrin-based pathways: metazoan inventions for integrating cells into tissues. Physiol Rev 81:1353–1392.

Berghs S, Aggujaro D, Dirkx R, Maksimova E, Stabach P, Hermel JM, Zhang JP, Philbrick W, Slepnev V, Ort T, Solimena M (2000) BetaIV spectrin, a new spectrin localized at axon initial segments and nodes of Ranvier in the central and peripheral nervous system. J Cell Biol 151:985–1002.

Berthold C-H (1978) Morphology of normal peripheral axons. In: Physiology and pathobiology of axons (Waxman SG, ed), pp 3–63. New York: Raven.

Bhat MA, Rios JC, Lu Y, Garcia-Fresco GP, Ching W, St Martin M, Li J, Einheber S, Chesler M, Rosenbluth J, Salzer JL, Bellen HJ (2001) Axon-glia interactions and the domain organization of myelinated axons requires neurexin IV/Caspr/Paranodin. Neuron 30:369–383.

Boiko T, Rasband MN, Levinson SR, Caldwell JH, Mandel G, Trimmer JS, Matthews G (2001) Compact myelin dictates the differential targeting of two sodium channel isoforms in the same axon. Neuron 30:91–104.

Boyle ME, Berglund EO, Murai KK, Weber L, Peles E, Ranscht B (2001) Contactin orchestrates assembly of the septate-like junctions at the paranode in myelinated peripheral nerve. Neuron 30:385–397.

Caldwell JH, Schaller KL, Lasher RS, Peles E, Levinson SR (2000) Sodium channel $Na_v1.6$ is localized at nodes of ranvier, dendrites, and synapses. Proc Natl Acad Sci USA 97:5616–5620.

Craner MJ, Lo AC, Black JA, Waxman SG (2003) Abnormal sodium channel distribution in optic nerve axons in a model of inflammatory demyelination. Brain 126:1552–1561.

de Medinaceli L, Freed WJ, Wyatt RJ (1982) An index of the functional condition of rat sciatic nerve based on measurements made from walking tracks. Exp Neurol 77:634–643.

de Waegh SM, Lee VM, Brady ST (1992) Local modulation of neurofilament phosphorylation, axonal caliber, and slow axonal transport by myelinating Schwann cells. Cell 68:451–463.

Delaunay J (2002) Molecular basis of red cell membrane disorders. Acta Haematol 108:210–218.

Devaux J, Alcaraz G, Grinspan J, Bennett V, Joho R, Crest M, Scherer SS (2003) Kv3.1b is a novel component of CNS nodes. J Neurosci 23:4509–4518.

Devaux JJ, Kleopa KA, Cooper EC, Scherer SS (2004) KCNQ2 is a nodal K^+ channel. J Neurosci 24:1236–1244.

Dupree JL, Girault J-A, Popko B (1999) Axo-glial interactions regulate the localization of axonal paranodal proteins. J Cell Biol 147:1145–1151.

Elder GA, Friedrich Jr VL, Margita A, Lazzarini RA (1999) Age-related atrophy of motor axons in mice deficient in the mid-sized neurofilament subunit. J Cell Biol 146:181–192.

Garcia ML, Lobsiger CS, Shah SB, Deerinck TJ, Crum J, Young D, Ward CM, Crawford TO, Gotow T, Uchiyama Y, Ellisman MH, Calcutt NA, Cleveland DW (2003) NF-M is an essential target for the myelin-directed "outside-in" signaling cascade that mediates radial axonal growth. J Cell Biol 163:1011–1020.

Gatto CL, Walker BJ, Lambert S (2003) Local ERM activation and dynamic growth cones at Schwann cell tips implicated in efficient formation of nodes of Ranvier. J Cell Biol 162:489–498.

Gong B, Rhodes KJ, Bekele-Arcuri Z, Trimmer JS (1999) Type I and type II Na^+ channel alpha-subunit polypeptides exhibit distinct spatial and temporal patterning, and association with auxiliary subunits in rat brain. J Comp Neurol 412:342–352.

Goutebroze L, Carnaud M, Denisenko N, Boutterin MC, Girault JA (2003) Syndecan-3 and syndecan-4 are enriched in Schwann cell perinodal processes. BMC Neurosci 4:29.

Jenkins SM, Bennett V (2001) Ankyrin-G coordinates assembly of the spectrin-based membrane skeleton, voltage-gated sodium channels, and L1 CAMs at Purkinje neuron initial segments. J Cell Biol 155:739–746.

Jenkins SM, Bennett V (2002) Developing nodes of Ranvier are defined by ankyrin-G clustering and are independent of paranodal axoglial adhesion. Proc Natl Acad Sci USA 99:2303–2308.

Kim HA, Zhang D, Stiles CD (2002) Signal requirements for wallerian degeneration revealed in a neuron-Schwann cell co-culture system. Soc Neurosci Abstr 28:819.13.

Komada M, Soriano P (2002) [Beta]IV-spectrin regulates sodium channel clustering through ankyrin-G at axon initial segments and nodes of Ranvier. J Cell Biol 156:337–348.

Lambert S, Davis JQ, Bennett V (1997) Morphogenesis of the node of Ranvier: co-clusters of ankyrin and ankyrin-binding integral proteins define early developmental intermediates. J Neurosci 17:7025–7036.

Lemaillet G, Walker B, Lambert S (2003) Identification of a conserved ankyrin-binding motif in the family of sodium channel alpha subunits. J Biol Chem 278:27333–27339.

Lemmon MA, Ferguson KM, Abrams CS (2002) Pleckstrin homology domains and the cytoskeleton. FEBS Lett 513:71–76.

Marchesi VT, Steers Jr E (1968) Selective solubilization of a protein component of the red cell membrane. Science 159:203–204.

Melendez-Vasquez CV, Rios JC, Zanazzi G, Lambert S, Bretscher A, Salzer JL (2001) Nodes of Ranvier form in association with ezrin-radixin-moesin (ERM)-positive Schwann cell processes. Proc Natl Acad Sci USA 98:1235–1240.

Nakada C, Ritchie K, Oba Y, Nakamura M, Hotta Y, Iino R, Kasai RS, Yamaguchi K, Fujiwara T, Kusumi A (2003) Accumulation of anchored proteins forms membrane diffusion barriers during neuronal polarization. Nat Cell Biol 5:626–632.

Ozmen S, Ayhan S, Latifoglu O, Siemionow M (2002) Stamp and paper method: a superior technique for the walking track analysis. Plast Reconstr Surg 109:1760–1761.

Parkinson NJ, Olsson CL, Hallows JL, McKee-Johnson J, Keogh BP, Noben-Trauth K, Kujawa SG, Tempel BL (2001) Mutant beta-spectrin 4 causes auditory and motor neuropathies in quivering mice. Nat Genet 29:61–65.

Peles E, Nativ M, Lustig M, Grumet M, Schilling J, Martinez R, Plowman GD, Schlessinger J (1997) Identification of a novel contactin-associated transmembrane receptor with multiple domains implicated in protein-protein interactions. EMBO J 16:978–988.

Poliak S, Peles E (2003) The local differentiation of myelinated axons at nodes of Ranvier. Nat Rev Neurosci 4:968–980.

Rao MV, Campbell J, Yuan A, Kumar A, Gotow T, Uchiyama Y, Nixon RA (2003) The neurofilament middle molecular mass subunit carboxyl-terminal tail domains is essential for the radial growth and cytoskeletal architecture of axons but not for regulating neurofilament transport rate. J Cell Biol 163:1021–1031.

Rasband MN, Trimmer JS (2001) Subunit composition and novel localization of K^+ channels in spinal cord. J Comp Neurol 429:166–176.

Rasband MN, Peles E, Trimmer JS, Levinson SR, Lux SE, Shrager P (1999) Dependence of nodal sodium channel clustering on paranodal axoglial contact in the developing CNS. J Neurosci 19:7516–7528.

Rasband MN, Taylor CM, Bansal R (2003a) Paranodal transverse bands are required for maintenance but not initiation of Nav1.6 sodium channel clustering in CNS optic nerve axons. Glia 44:173–182.

Rasband MN, Kagawa T, Park EW, Ikenaka K, Trimmer JS (2003b) Dysregulation of axonal sodium channel isoforms after adult-onset chronic demyelination. J Neurosci Res 73:465–470.

Rhodes KJ, Keilbaugh SA, Barrezueta NX, Lopez KL, Trimmer JS (1995) Association and colocalization of K^+ channel α- and β-subunit polypeptides in rat brain. J Neurosci 15:5360–5371.

Rios JC, Rubin M, St Martin M, Downey RT, Einheber S, Rosenbluth J, Levinson SR, Bhat M, Salzer JL (2003) Paranodal interactions regulate

expression of sodium channel subtypes and provide a diffusion barrier for the node of Ranvier. J Neurosci 23:7001–7011.

Saito F, Moore SA, Barresi R, Henry MD, Messing A, Ross-Barta SE, Cohn RD, Williamson RA, Sluka KA, Sherman DL, Brophy PJ, Schmelzer JD, Low PA, Wrabetz L, Feltri ML, Campbell KP (2003) Unique role of dystroglycan in peripheral nerve myelination, nodal structure, and sodium channel stabilization. Neuron 38:747–758.

Salzer JL (2003) Polarized domains of myelinated axons. Neuron 40:297–318.

Schafer DP, Bansal R, Hedstrom KL, Pfeiffer SE, Rasband MN (2004) Does paranode formation and maintenance require partitioning of Neurofascin 155 into lipid rafts? J Neurosci 24:3176–3185.

Scherer SS, Xu T, Crino P, Arroyo EJ, Gutmann DH (2001) Ezrin, radixin, and moesin are components of Schwann cell microvilli. J Neurosci Res 65:150–164.

Trapp BD, Andrews SB, Wong A, O'Connell M, Griffin JW (1989) Co-localization of the myelin-associated glycoprotein and the microfilament components, F-actin and spectrin, in Schwann cells of myelinated nerve fibres. J Neurocytol 18:47–60.

Tse WT, Tang J, Jin O, Korsgren C, John KM, Kung AL, Gwynn B, Peters LL, Lux SE (2001) A new spectrin, beta IV, has a major truncated isoform that associates with promyelocytic leukemia protein nuclear bodies and the nuclear matrix. J Biol Chem 276:23974–23985.

Wang H, Kunkel DD, Martin TM, Schwartzkroin PA, Tempel BL (1993) Heteromultimeric K^+ channels in terminal and juxtaparanodal regions of neurons. Nature 365:75–79.

Westenbroek RE, Noebels JL, Catterall WA (1992) Elevated expression of type II Na^+ channels in hypomyelinated axons of shiverer mouse brain. J Neurosci 12:2259–2267.

Zhou D, Lambert S, Malen PL, Carpenter S, Boland LM, Bennett V (1998) AnkyrinG is required for clustering of voltage-gated Na channels at axon initial segments and for normal action potential firing. J Cell Biol 143:1295–1304.